15th IFK
Proc. of the 15th International Fluid Power Conference <Symposium/Conference>
<DOI>

Multidimensional Neural Networks Based RISE Control for Hydraulic Manipulators with Disturbances Compensation

Junjie Mi[1], Gang Shen[1], Jianyong Yao[2]

1. School of Mechatronics Engineering, Anhui University of Science & Technology, Huainan, Anhui 232001, China, mijunjie@aust.edu.cn, 2023020@aust.edu.cn

2. School of Mechanical Engineering, Nanjing University of Science & Technology, Nanjing, Jiangsu 210094, China, yaojianyong@njust.edu.cn

Abstract.

With the accelerated development of automation and unmanned operations in heavy-load engineering fields, higher demands are placed on the control performance of hydraulically driven heavy-load manipulators. However, hydraulic manipulators suffer from prominent issues such as large load fluctuations, significant dynamic model errors, and strong joint coupling characteristics, which readily lead to degraded control performance. To achieve high-precision pose control, this study proposes a nonlinear disturbances compensation controller. A multidimensional radial basis function neural network (mRBFNN) is used to approximate various uncertain nonlinearities present in the system. Combined with the backstepping method, a nonlinear robust integral of the sign of the error (RISE) controller is designed. Online compensation for uncertain nonlinearities is realized during the control law design process, thereby enhancing system robustness. The Lyapunov stability theory proves that the system is stable and all signals are bounded. Simulation results demonstrate that the proposed control strategy significantly improves joint tracking accuracy and anti-disturbance capability of the hydraulically driven manipulator, fully validating the effectiveness of the control strategy.

Keywords. Hydraulic manipulator, Electro-hydraulic servo system, Multidimensional radial basis function neural network (mRBFNN), Disturbances compensation.

1. INTRODUCTION

In fields such as heavy equipment, hydraulic systems play an irreplaceable role[1]. However, hydraulic systems inherently possess strong nonlinearity, time-varying parameters, and sensitivity to external disturbances, posing significant challenges to achieving high-precision control[2]. In recent years, with the rapid development of nonlinear control theory, combining advanced control strategies with the characteristics of hydraulic systems to achieve high dynamic performance control for multi-degree-of-freedom (DOF) hydraulic manipulators has become a hot topic of common interest in academia and industry[3].

In the field of nonlinear control theory, methods such as sliding mode control, adaptive control, and robust control have been widely applied in hydraulic systems[4][5]. However, most current research focuses on single-DOF systems, leaving room for improvement in handling the coupled nonlinearities of multi-DOF hydraulic manipulators[6].

In recent years, significant progress has been made in the field of fluid power transmission and control regarding hydraulic system modeling and compensation. Liu et al.[7] proposed a model predictive control based on a state observer for large-scale offshore hydraulic systems, laying a foundation for high-precision control of hydraulic systems under complex working conditions. Literature[8][9] published in the journal Chinese Hydraulics & Pneumatics proposed compensation strategies for the nonlinear flow characteristics and pressure dynamics of valve-controlled asymmetric cylinders, respectively. Notably, Xia et al.[10] experimentally verified the good effect of friction compensation on improving the low-speed performance of hydraulic systems. Regarding parameter identification, intelligent algorithms such as particle swarm optimization[11] and deep reinforcement learning[12] have been introduced to improve model accuracy. However, most existing compensation methods rely on accurate system models, and their adaptability to parameter variations in multi-DOF systems needs further enhancement.

Traditional PID control is still widely used in industry due to its simple structure and few adjustable parameters, but its performance is limited when dealing with the nonlinear coupling characteristics of hydraulic manipulators. To address this issue, scholars have proposed various solutions: Yao et al.[13] designed an adaptive robust controller to handle model uncertainties; Chen et al.[14] combined a disturbance observer with the backstepping method to suppress the effects of external disturbances. In the study of manipulator trajectory tracking, Zhu et al.[15] verified the advantage of prescribed performance control in constraining tracking errors, but this study did not consider the dynamic characteristics of hydraulic actuators.

The remaining sections of this study are arranged as follows: Section 1 introduces the nonlinear mathematical model of the hydraulic manipulator; Section 2 details the design method of the multidimensional neural network; Section 3 presents the design process of the nonlinear integral robust controller; Section 4 verifies the effectiveness of the proposed algorithm through simulation examples; Section 5 summarizes the research.

2. NONLINEAR MATHEMATICAL MODEL OF THE HYDRAULIC MANIPULATOR

2.1. Dynamic Model of the Hydraulic Manipulator

Using the Lagrange energy method, the dynamic equation for a multi-DOF manipulator can be formulated as follows

$$\boldsymbol{\tau}=\boldsymbol{M}(\boldsymbol{y})\ddot{\boldsymbol{y}}+\boldsymbol{C}(\boldsymbol{y},\dot{\boldsymbol{y}})\dot{\boldsymbol{y}}+\boldsymbol{G}(\boldsymbol{y})+\boldsymbol{\Delta}_{t1}(t) \tag{1}$$

where $\boldsymbol{M}(\boldsymbol{y})\in\mathbb{R}^{n\times n}$ is the manipulator's mass matrix, which is positive definite and symmetric. Its off-diagonal elements $M_{ij}=M_{ji}$ represent force coupling effects between joints. $\boldsymbol{C}(\boldsymbol{y},\dot{\boldsymbol{y}})\in\mathbb{R}^{n\times n}$ represents the Coriolis and centrifugal force matrix, describing the coupling between joint velocities and forces. $\boldsymbol{G}(\boldsymbol{y})\in\mathbb{R}^{n}$ is the gravity vector. $\boldsymbol{\Delta}_{t1}(t)\in\mathbb{R}^{n}$ represents unmodeled uncertainties in the manipulator's dynamic model, such as link elasticity, joint clearance, and connection relationships. $\boldsymbol{y}=[y_1,...,y_n]^{\mathrm{T}}\in\mathbb{R}^{n}$ represents the rotation angle of each joint.

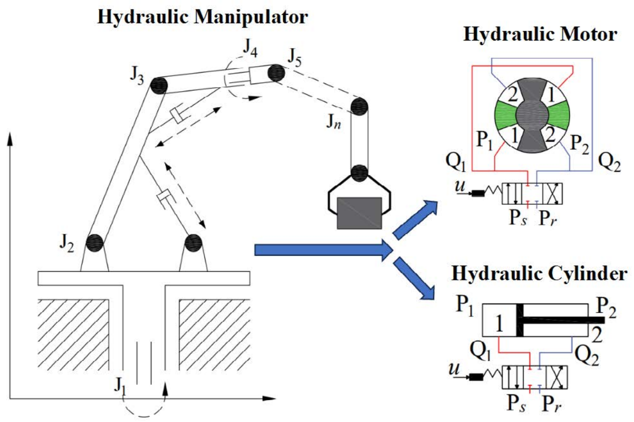

Figure 1 Configuration Diagram and Actuator of m-DOF Hydraulic Manipulator

As shown in Figure 1, hydraulic motors and hydraulic cylinders are responsible for driving different joints. The hydraulic cylinder is a single-rod cylinder, where 1 denotes the rodless chamber and 2 denotes the rod chamber. The hydraulic motor is a rotary actuator, with its position controlled by regulating the flow into and out of its ports via a servovalve.

Assumption 1: The servovalve's orifices are considered symmetric, and its dynamics are simplified as a proportional element.

Assumption 2: Considering the compact layout of the device and oil source, the oil in different chambers is assumed to have the same bulk modulus.

To maintain generality, the pressure dynamics of the electro-hydraulic servo system can be described as:

$$\begin{cases}\dot{p}_{1i}=\beta_{\mathrm{e}}V_{1i}^{-1}\left(q_{1i}-A_{1i}\dot{x}_{si}-C_{\mathrm{t}}\left(\dot{p}_{1i}-\dot{p}_{2i}\right)\right)+d_{1i}(t)\\ \dot{p}_{2i}=\beta_{\mathrm{e}}V_{2i}^{-1}\left(-q_{2i}-A_{2i}\dot{x}_{si}+C_{\mathrm{t}}\left(\dot{p}_{1i}-\dot{p}_{2i}\right)\right)-d_{2i}(t)\end{cases} \tag{2}$$

$$\begin{cases} V_{1i} = V_{01i} + A_{1i} x_{si} \\ V_{2i} = V_{02i} - A_{2i} x_{si} \end{cases} \tag{3}$$

where the subscript i denotes different joint numbers, $i = 1,2,...,n$; β_e represents the bulk modulus of the hydraulic oil, assumed constant; x_{si} represents the displacement of the actuator driving the joint. For a hydraulic motor, this is the joint rotation angle; for a hydraulic cylinder, it is the piston displacement. A_{1i} and A_{2i} are the effective areas of the piston or motor vane; V_{01i} and V_{02i} represent the initial volumes of the two chambers; V_{1i} and V_{2i} represent the actual volumes of the two chambers during motion; p_{1i} and p_{2i} represent the pressures in the two chambers; q_{1i} and q_{2i} denote the flow rates into/out of the two chambers; C_t is the internal leakage coefficient; $d_{1i}(t)$ and $d_{2i}(t)$ represent unmodeled uncertainties and external leakage in the pressure dynamics model.

The servovalve adjusts the orifice opening by changing the spool position, thereby regulating the flow into and out of the actuator chambers. The servovalve flow equation can be expressed as:

$$\begin{cases} q_{1i} = k_{qi} x_{vi} \left(s(x_{vi}) \sqrt{p_s - p_{1i}} + s(x_{vi}) \sqrt{p_{1i} - p_r} \right) \\ q_{2i} = k_{qi} x_{vi} \left(s(x_{vi}) \sqrt{p_{2i} - p_r} + s(x_{vi}) \sqrt{p_s - p_{2i}} \right) \end{cases} \tag{4}$$

$$k_{qi} = C_{di} w_i \sqrt{2/\rho_i}, \qquad x_{vi} = k_{ui} u_i \tag{5}$$

where k_{qi} represents the flow gain for the left and right spool displacements of the servovalve; p_s is the supply pressure, p_r is the return pressure; x_{vi} is the servovalve spool displacement; C_{di} is the flow coefficient of the servovalve orifice; w_i is the area gradient of the orifice; ρ is the density of the hydraulic oil. The function $s(*)$ is defined as:

$$s(*) = \begin{cases} 1, & \text{if } * \geq 0 \\ 0, & \text{if } * < 0 \end{cases} \tag{6}$$

Therefore, the flow equation (4) of the electro-hydraulic servo system can be rewritten as:

$$\begin{cases} q_{1i} = k_{ti} R_{1i} u_i \\ q_{2i} = k_{ti} R_{2i} u_i \end{cases} \tag{7}$$

where $k_{ti} = k_{qi} k_{ui}$. Also:

$$\begin{cases} R_{1i} = s(u_i) \sqrt{p_s - p_{1i}} + s(u_i) \sqrt{p_{1i} - p_r} \\ R_{2i} = s(u_i) \sqrt{p_s - p_{1i}} + s(u_i) \sqrt{p_{1i} - p_r} \end{cases} \tag{8}$$

The actual output force/torque of the electro-hydraulic servo system can be expressed as:

2.2. Linear-to-Rotational Nonlinear Transformation of the Actuator

The actuators of the multi-DOF hydraulic manipulator primarily consist of valve-controlled hydraulic cylinders and hydraulic motors. Two hydraulic cylinders are responsible for driving the joints with larger loads (joints 2 and 3), involving a nonlinear transformation from linear to rotational motion, i.e., a structural nonlinear relationship exists.

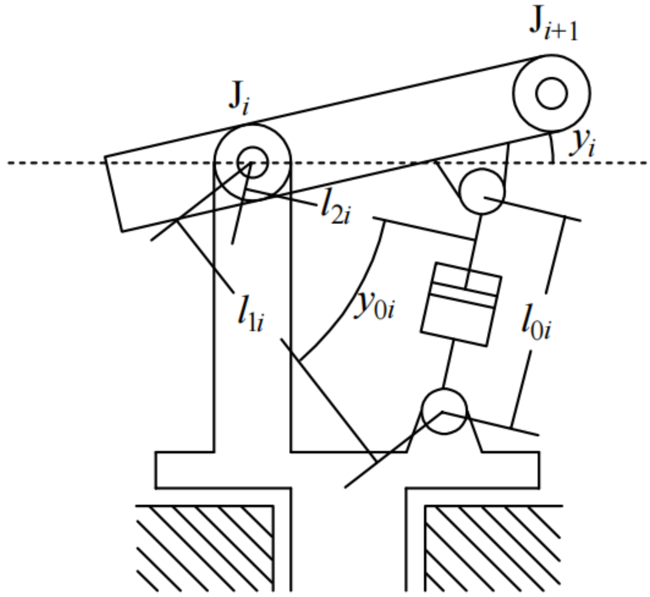

Figure 2 Schematic Diagram of Joint Linear-to-Rotational Nonlinear Transformation

The structural nonlinearity of the hydraulic manipulator is shown in Figure 2, where a hydraulic cylinder pushes a load to rotate about a pivot. Here, y_i represents the initial angle between the driven link and the horizontal plane; y_{0i} represents the initial angle between the two pivot points of the cylinder and the link's rotation axis; l_{1i} is the distance from the fixed pivot of the cylinder to the link's rotation axis; l_{2i} is the distance from the moving pivot of the cylinder to the link's rotation axis; l_{0i} is the initial length of the cylinder.

Based on the geometric relationships and the law of cosines, we obtain:

$$l_i = \sqrt{l_{1i}^2 + l_{2i}^2 - 2l_{1i}l_{2i}\cos\left(y_{0i} + y_i\right)} \tag{9}$$

Let the actual displacement of the cylinder be $x_{\mathrm{p}i} = l_i - l_{0i}$. Thus, the actual velocity of the cylinder is:

$$\begin{aligned} v_{\mathrm{p}i} = \dot{x}_{\mathrm{p}i} &= \frac{\mathrm{d}\left(l_i - l_{0i}\right)}{\mathrm{d}t} = \frac{\mathrm{d}l_i}{\mathrm{d}t} \\ &= \frac{l_{1i}l_{2i}\sin\left(y_{0i} + y_i\right)}{\sqrt{l_{1i}^2 + l_{2i}^2 - 2l_{1i}l_{2i}\cos\left(y_{0i} + y_i\right)}}\dot{y}_i \\ &= S_i\left(y_i\right)\dot{y}_i \end{aligned} \tag{10}$$

where $S_i\left(y_i\right)$ is also the perpendicular distance from the cylinder to the link's rotation axis.

Based on the above analysis, x_{si} in Eq. (3) can be expressed as:

$$x_{si} = \begin{cases} y_i & \text{,driven by motor} \\ \sqrt{l_{1i}^2 + l_{2i}^2 - 2l_{1i}l_{2i}\cos\left(y_{0i} + y_i\right)} - l_{0i} & \text{,driven by cylinder} \end{cases} \tag{11}$$

The actuator's own velocity can be obtained from Eq. (11):

$$\dot{x}_{si} = S_i\left(y_i\right)\dot{y}_i \tag{12}$$

$$S_i(y_i)=\begin{cases}1 & \text{,driven by motor}\\ \dfrac{l_{1i}l_{2i}\sin(y_{0i}+y_i)}{\sqrt{l_{1i}^2+l_{2i}^2-2l_{1i}l_{2i}\cos(y_{0i}+y_i)}} & \text{,driven by cylinder}\end{cases} \tag{13}$$

Combining Eq. (9), the actual output torque of the manipulator actuator for each joint can be expressed as:

$$T_i=S_i(y_i)(A_{1i}p_{1i}-A_{2i}p_{2i}) \tag{14}$$

2.3. *State-Space Equation of the Hydraulic Manipulator*

To facilitate subsequent controller design and analysis, define the state variables $\boldsymbol{x}=[\boldsymbol{x}_1^{\mathrm{T}},\boldsymbol{x}_2^{\mathrm{T}},\boldsymbol{x}_3^{\mathrm{T}}]^{\mathrm{T}}$, $\boldsymbol{x}_1=\boldsymbol{y}=[y_1,y_2,\cdots,y_n]^{\mathrm{T}}$, $\boldsymbol{x}_2=\dot{\boldsymbol{x}}_1=[\dot{y}_1,\dot{y}_2,\cdots,\dot{y}_n]^{\mathrm{T}}$, $\boldsymbol{x}_3=\boldsymbol{A}_1\boldsymbol{p}_1-\boldsymbol{A}_2\boldsymbol{p}_2$. Define the manipulator's time-varying rotation angle and angular velocity as y_i and $\dot{y}_i$, respectively. Combining the above equations, the nonlinear dynamic model of the multi-DOF hydraulic manipulator can be expressed in state-space form as:

$$\begin{aligned}&\dot{\boldsymbol{x}}_1=\boldsymbol{x}_2\\&\dot{\boldsymbol{x}}_2=\boldsymbol{M}^{-1}(\boldsymbol{x}_1)\left[\boldsymbol{S}(\boldsymbol{x}_1)\boldsymbol{x}_3-\boldsymbol{G}(\boldsymbol{x}_1)-\boldsymbol{C}(\boldsymbol{x}_1,\boldsymbol{x}_2)\boldsymbol{x}_2\right]\\&\qquad+\boldsymbol{M}^{-1}(\boldsymbol{x}_1)\boldsymbol{\Delta}_{t1}\\&\dot{\boldsymbol{x}}_3=\boldsymbol{f}_1\boldsymbol{u}-\boldsymbol{f}_2-\boldsymbol{f}_3+\boldsymbol{\Delta}_{t2}\end{aligned} \tag{15}$$

where the control input vector for each joint's actuator in the hydraulic manipulator system is $\boldsymbol{u}=[u_1,u_2,\cdots,u_n]^{\mathrm{T}}$; expressions for other vectors can be found in [16].

Assumption 3: The commanded trajectory $\boldsymbol{x}_{1d}=[x_{11d},x_{12d},\cdots,x_{1nd}]^{\mathrm{T}}$ for each joint of the hydraulic manipulator is third-order differentiable, and all its derivatives are bounded.

Assumption 4: The elements of the unmatched uncertainty $\boldsymbol{\Delta}_{t1}=[\Delta_{t11},\Delta_{t12},\cdots,\Delta_{t1n}]^{\mathrm{T}}$ and the matched uncertainty $\boldsymbol{\Delta}_{t2}=[\Delta_{t21},\Delta_{t22},\cdots,\Delta_{t2n}]^{\mathrm{T}}$ are sufficiently smooth, and their first and second derivatives exist and are bounded.

3. MULTIDIMENSIONAL NEURAL NETWORK DESIGN

For hydraulic manipulators, complex joint coupling and unmodeled uncertainties are the main factors affecting high-precision position tracking. Therefore, this section employs a multidimensional radial basis function neural networks (mRBFNNs) to approximate and estimate the uncertain joint coupling dynamics and unmodeled disturbances of the hydraulic manipulator, achieving feedforward compensation during the controller design process.

From (16), it can be seen that $\boldsymbol{\Delta}_{t1}$ is related to the position, velocity, and acceleration signals of each joint, while $\boldsymbol{\Delta}_{t2}$ is only related to joint positions. Therefore, $\boldsymbol{\Delta}_{t1}$ and $\boldsymbol{\Delta}_{t2}$ can be designed in the following form:

$$\boldsymbol{\Delta}_{t1}=\left[\boldsymbol{W}_{11}^{\mathrm{T}}\boldsymbol{h}_{11}(\boldsymbol{\chi}_1),\cdots,\boldsymbol{W}_{1n}^{\mathrm{T}}\boldsymbol{h}_{1n}(\boldsymbol{\chi}_n)\right]^{\mathrm{T}}+\boldsymbol{\varepsilon}_1 \tag{16}$$

$$\boldsymbol{\Delta}_{t2}=\left[\boldsymbol{W}_{21}^{\mathrm{T}}\boldsymbol{h}_{21}(y_1),\cdots,\boldsymbol{W}_{2n}^{\mathrm{T}}\boldsymbol{h}_{2n}(y_n)\right]^{\mathrm{T}}+\boldsymbol{\varepsilon}_2 \tag{17}$$

where $\boldsymbol{W}_{1i}=[W_{1i1},\cdots,W_{1iH}]^{\mathrm{T}}\in\mathbb{R}^H$, H represent the number of neurons in the first neural network hidden layer; $\boldsymbol{W}_{2i}=[W_{2i1},\cdots,W_{2iL}]^{\mathrm{T}}\in\mathbb{R}^L$, L represent the number of neurons in the second neural network hidden layer; $\boldsymbol{\chi}_i = [1, y_i, \dot{y}_i, \ddot{y}_i]^{\mathrm{T}}$ is the input signal to the first neural network; $\boldsymbol{\varepsilon}_i = [\varepsilon_{i1}, \cdots, \varepsilon_{in}]^{\mathrm{T}} \in \mathbb{R}^n$ represents the function reconstruction error; $\boldsymbol{h}_{1i} = [h_{1i1}, \cdots, h_{1iH}]^{\mathrm{T}} \in \mathbb{R}^H$ and $\boldsymbol{h}_{2i} = [h_{2i1}, \cdots, h_{2iL}]^{\mathrm{T}} \in \mathbb{R}^L$ are the Gaussian radial basis functions for the two different neural networks, expressed as follows:

$$h_{1ij} = \exp\left(-\frac{\left\| \boldsymbol{\chi}_i - \sigma_{1j} I_4 \right\|^2}{2\iota_{1j}} \right), \quad \begin{cases} i = 1, 2, \cdots, n \\ j = 1, 2, \cdots, H \end{cases} \tag{18}$$

$$h_{2ij} = \exp\left(-\frac{\left(y_i - \sigma_{2j} \right)^2}{2\iota_{2j}} \right), \quad \begin{cases} i = 1, 2, \cdots, n \\ j = 1, 2, \cdots, L \end{cases} \tag{19}$$

where $\boldsymbol{\sigma}_1 = \left[\sigma_{1j}, \cdots, \sigma_{1H} \right]^{\mathrm{T}}$ and $\boldsymbol{\sigma}_2 = \left[\sigma_{2j}, \cdots, \sigma_{2L} \right]^{\mathrm{T}}$ represent acceptable center ranges; $\boldsymbol{\iota}_1 = \left[\iota_{1j}, \cdots, \iota_{1H} \right]^{\mathrm{T}}$ and $\iota_2 = \left[\iota_{2j}, \cdots, \iota_{2L} \right]^{\mathrm{T}}$ represent the widths of the Gaussian functions.

Assumption 5: The function reconstruction error $\boldsymbol{\varepsilon}_i = [\varepsilon_{i1}, \cdots, \varepsilon_{in}]^{\mathrm{T}}$ and its second derivative with respect to time are bounded:

$$\begin{cases} \left\| \boldsymbol{\varepsilon}_1 \right\| \le \varepsilon_{1d1}, \ \left\| \dot{\boldsymbol{\varepsilon}}_1 \right\| \le \varepsilon_{1d2}, \ \left\| \ddot{\boldsymbol{\varepsilon}}_1 \right\| \le \varepsilon_{1d3} \\ \left\| \boldsymbol{\varepsilon}_2 \right\| \le \varepsilon_{2d1}, \ \left\| \dot{\boldsymbol{\varepsilon}}_2 \right\| \le \varepsilon_{2d2}, \ \left\| \ddot{\boldsymbol{\varepsilon}}_2 \right\| \le \varepsilon_{2d3} \end{cases} \tag{20}$$

where ε_{id1}, ε_{id2}, and ε_{id3} are positive constants.

Considering that increasing the number of neural network hidden layers and manipulator joints makes tuning the weight matrices $\boldsymbol{W}_{1i}$ and $\boldsymbol{W}_{2i}$ extremely difficult, this study introduces an adaptive method for self-tuning the weight matrices. Based on (17) and (18), their adaptive approximation expressions can be obtained as follows:

$$\hat{\boldsymbol{\Delta}}_{t1} = \left[\hat{\boldsymbol{W}}_{11}^{\mathrm{T}} \boldsymbol{h}_{11}(\boldsymbol{\chi}_1), \cdots, \hat{\boldsymbol{W}}_{1n}^{\mathrm{T}} \boldsymbol{h}_{1n}(\boldsymbol{\chi}_n) \right]^{\mathrm{T}} \tag{21}$$

$$\hat{\boldsymbol{\Delta}}_{t2} = \left[\hat{\boldsymbol{W}}_{21}^{\mathrm{T}} \boldsymbol{h}_{21}(y_1), \cdots, \hat{\boldsymbol{W}}_{2n}^{\mathrm{T}} \boldsymbol{h}_{2n}(y_n) \right]^{\mathrm{T}} \tag{22}$$

where $\hat{\boldsymbol{W}}_{1i} = \left[\hat{W}_{1i1}, \cdots, \hat{W}_{1iH} \right]^{\mathrm{T}} \in \mathbb{R}^H$ and $\hat{\boldsymbol{W}}_{2i} = \left[\hat{W}_{2i1}, \cdots, \hat{W}_{2iL} \right]^{\mathrm{T}} \in \mathbb{R}^L$ represent the estimated values of the ideal weights.

The adaptive laws for the neural network weights are as follows:

$$\begin{cases} \dot{\hat{\boldsymbol{W}}}_{1i} = \mathrm{sat}_{\hat{\boldsymbol{W}}_{1iM}} \left(\mathrm{Proj}_{\hat{\boldsymbol{W}}_{1i}} \left(\boldsymbol{\Gamma}_{1i} \boldsymbol{\tau}_{1i} \right) \right) \\ \dot{\hat{\boldsymbol{W}}}_{2i} = \mathrm{sat}_{\hat{\boldsymbol{W}}_{2iM}} \left(\mathrm{Proj}_{\hat{\boldsymbol{W}}_{2i}} \left(\boldsymbol{\Gamma}_{2i} \boldsymbol{\tau}_{2i} \right) \right) \end{cases} \tag{23}$$

$$\begin{cases} \boldsymbol{\tau}_{1i} = \boldsymbol{h}_{1i} z_{2i} \\ \boldsymbol{\tau}_{2i} = \boldsymbol{h}_{2i} z_{3i} \end{cases} \tag{24}$$

where $\boldsymbol{\Gamma}$ is a positive definite matrix determining the adaptive rate of the weights; $\boldsymbol{\tau}$ is defined as the adaptive function for the neural network weights; other function definitions are as shown in [17].

Define the estimation errors as follows:

$$\tilde{\bullet} = \bullet - \hat{\bullet} \tag{25}$$

According to (22), define the following variables:

$$\tilde{\boldsymbol{\Delta}}_{t1} = \left[\tilde{\boldsymbol{W}}_{11}^{\mathrm{T}} \boldsymbol{h}_{11}(\boldsymbol{\chi}_1), \cdots, \tilde{\boldsymbol{W}}_{1n}^{\mathrm{T}} \boldsymbol{h}_{1n}(\boldsymbol{\chi}_n) \right]^{\mathrm{T}} \tag{26}$$

$$\tilde{\mathbf{\Delta}}_{tw1} = \left[\dot{\tilde{\boldsymbol{W}}}_{11}^{\mathrm{T}} \boldsymbol{h}_{11}\left(\chi_1\right), \cdots, \dot{\tilde{\boldsymbol{W}}}_{1n}^{\mathrm{T}} \boldsymbol{h}_{1n}\left(\chi_n\right) \right]^{\mathrm{T}} \tag{27}$$

$$\tilde{\mathbf{\Delta}}_{th1} = \left[\tilde{\boldsymbol{W}}_{11}^{\mathrm{T}} \dot{\boldsymbol{h}}_{11}\left(\chi_1\right), \cdots, \tilde{\boldsymbol{W}}_{1n}^{\mathrm{T}} \dot{\boldsymbol{h}}_{1n}\left(\chi_n\right) \right]^{\mathrm{T}} \tag{28}$$

To simplify the proof process, the transformed form of (23) follows the same principle.

4. Controller Design and Stability Analysis

4.1. *Nonlinear Integral Robust Controller Design*

Define the error variable vectors as follows:

$$\begin{cases} \boldsymbol{z}_1 = \boldsymbol{x}_1 - \boldsymbol{x}_{1d} \\ \boldsymbol{z}_2 = \dot{\boldsymbol{z}}_1 + \boldsymbol{k}_1 \boldsymbol{z}_1 \\ \boldsymbol{z}_3 = \boldsymbol{x}_3 - \boldsymbol{\alpha}_2 \\ \boldsymbol{r}_1 = \dot{\boldsymbol{z}}_2 + \boldsymbol{k}_2 \boldsymbol{z}_2 \\ \boldsymbol{r}_2 = \dot{\boldsymbol{z}}_3 + \boldsymbol{k}_3 \boldsymbol{z}_3 \end{cases} \tag{29}$$

where $\boldsymbol{r}_1$ and $\boldsymbol{r}_2$ are auxiliary error variable vectors, which can help suppress matched and unmatched uncertainties during controller design; $\boldsymbol{k}_1 = \mathrm{diag}\{k_{11}, k_{12}, \cdots, k_{1n}\}$, $\boldsymbol{k}_2 = \mathrm{diag}\{k_{21}, k_{22}, \cdots, k_{2n}\}$, $\boldsymbol{k}_3 = \mathrm{diag}\{k_{31}, k_{32}, \cdots, k_{3n}\}$ represent tunable controller gain matrices.

Based on the above equation, the virtual control law https://media/image111.wmf can be designed as follows:

$$\begin{aligned} \boldsymbol{\alpha}_2 &= \boldsymbol{S}^{-1}\left(\boldsymbol{x}_1\right)\left[\boldsymbol{\alpha}_{2a} + \boldsymbol{\alpha}_{2s1} + \boldsymbol{\alpha}_{2s2}\right] \\ \boldsymbol{\alpha}_{2a} &= \boldsymbol{G}\left(\boldsymbol{x}_1\right) + \boldsymbol{C}\left(\boldsymbol{x}_1, \boldsymbol{x}_2\right)\boldsymbol{x}_2 - \hat{\mathbf{\Delta}}_{t1} \\ &\quad + \boldsymbol{M}\left(\boldsymbol{x}_1\right)\ddot{\boldsymbol{x}}_{1d} \\ \boldsymbol{\alpha}_{2s1} &= -\left(\boldsymbol{k}_{r1} + \boldsymbol{k}_s\right)\boldsymbol{z}_2 - \boldsymbol{M}\left(\boldsymbol{x}_1\right)\boldsymbol{k}_1 \dot{\boldsymbol{z}}_1 - \boldsymbol{M}\left(\boldsymbol{x}_1\right)\boldsymbol{k}_2 \boldsymbol{z}_2 \\ \boldsymbol{\alpha}_{2s2} &= -\int_0^t \left[\left(\boldsymbol{k}_{r1} + \boldsymbol{k}_s\right)\boldsymbol{k}_2 \boldsymbol{z}_2 + \boldsymbol{\upsilon}\left(\boldsymbol{z}_2\right)\boldsymbol{\beta}_1\right]\mathrm{d}\tau \end{aligned} \tag{30}$$

where $\mathrm{sign}(*)$ represents the sign function; the sign function matrix $\boldsymbol{\upsilon}(\boldsymbol{z}_2)$ is $\boldsymbol{\upsilon}(\boldsymbol{z}_2) = \mathrm{diag}\{\mathrm{sign}(z_{21}), \cdots, \mathrm{sign}(z_{2n})\}$; the control gain is $\boldsymbol{k}_{r1} = \mathrm{diag}\{k_{r11}, k_{r12}, \cdots, k_{r1n}\}$, and all elements in the matrix are positive; $\boldsymbol{\beta}_1 = [\beta_{11}, \beta_{12}, \cdots, \beta_{1n}]^{\mathrm{T}}$ is a gain vector with all positive elements; $\boldsymbol{k}_s = \mathrm{diag}\{k_{s1}, k_{s2}, \cdots, k_{sn}\}$ is an auxiliary constant variable matrix with all elements being real numbers greater than 0.

The expanded form of the auxiliary error vector $\boldsymbol{r}_1$ is:

$$\boldsymbol{M}\left(\boldsymbol{x}_1\right)\dot{\boldsymbol{r}}_1 = \boldsymbol{S}\left(\boldsymbol{x}_1\right)\dot{\boldsymbol{z}}_3 - \left(\boldsymbol{k}_{r1} + \boldsymbol{k}_s\right)\boldsymbol{r}_1 - \boldsymbol{\upsilon}\left(\boldsymbol{z}_2\right)\boldsymbol{\beta}_1 + \boldsymbol{N}_1 \tag{31}$$

From (31), it is known that $\boldsymbol{N}_1$ is bounded. The bound of $\boldsymbol{N}_1$ can be expressed as:

$$\left\|\boldsymbol{N}_1\right\| \le \delta_1, \quad \left\|\dot{\boldsymbol{N}}_1\right\| \le \delta_2 \tag{32}$$

where δ_1 and δ_2 are constants greater than 0.

Based on the expansion of the auxiliary error function $\boldsymbol{r}_2$, the actual control law can be designed as follows:

$$\begin{aligned} \boldsymbol{u} &= \boldsymbol{f}_1^{-1}\left(\boldsymbol{u}_a + \boldsymbol{u}_{s1} + \boldsymbol{u}_{s2}\right) \\ \boldsymbol{u}_a &= \boldsymbol{f}_2 + \boldsymbol{f}_3 + \dot{\boldsymbol{\alpha}}_2 - \hat{\boldsymbol{\Delta}}_{t2} \\ \boldsymbol{u}_{s1} &= -\boldsymbol{k}_{r2}\boldsymbol{z}_3 - \boldsymbol{k}_3\boldsymbol{z}_3 \\ \boldsymbol{u}_{s2} &= -\int_0^t \left[\boldsymbol{k}_{r2}\boldsymbol{k}_3\boldsymbol{z}_3 + \boldsymbol{v}\left(\boldsymbol{z}_3\right)\boldsymbol{\beta}_2\right]\mathrm{d}\tau \end{aligned} \tag{33}$$

where $\boldsymbol{\beta}_2 = \left[\beta_{21}, \beta_{22}, \cdots, \beta_{2n}\right]^{\mathrm{T}}$ is a gain vector; $\boldsymbol{u}_a$ is the model compensation term; $\boldsymbol{u}_{s1}$ represents the linear feedback term for system tuning; the sign function matrix $\boldsymbol{v}\left(\boldsymbol{z}_3\right) = \mathrm{diag}\left\{\mathrm{sign}\left(z_{31}\right), \cdots, \mathrm{sign}\left(z_{3n}\right)\right\}$; $\boldsymbol{u}_{s2}$ is the system's RISE feedback term, which can suppress the influence of matched uncertainties on system control performance to some extent.

Combining the specific form of the actual control law in (42), the time derivative of $\boldsymbol{r}_2$ can be expanded as:

$$\dot{\boldsymbol{r}}_2 = -\boldsymbol{k}_{r2}\boldsymbol{r}_2 - \boldsymbol{v}\left(\boldsymbol{z}_3\right)\boldsymbol{\beta}_2 + \boldsymbol{N}_2 \tag{34}$$

From (34), it is known that $\boldsymbol{N}_2$ is bounded. The bound of $\boldsymbol{N}_2$ can be expressed as:

$$\left\|\boldsymbol{N}_2\right\| \le \xi_1, \quad \left\|\dot{\boldsymbol{N}}_2\right\| \le \xi_2 \tag{35}$$

where δ_1 and δ_2 are constants greater than 0.

4.2. *Controller Stability Analysis*

To analyze the controller's performance and stability, the following theorems are given.

Theorem 1: There always exist real vectors $\boldsymbol{\beta}_1 = \left[\beta_{11}, \beta_{12}, \cdots, \beta_{1n}\right]^{\mathrm{T}}$ and $\boldsymbol{\beta}_2 = \left[\beta_{21}, \beta_{22}, \cdots, \beta_{2n}\right]^{\mathrm{T}}$, whose elements always satisfy the following conditions:

$$\beta_{1i} \ge \delta_{1i} + \frac{1}{k_{2i}}\delta_{2i} \tag{36}$$

$$\beta_{2i} \ge \xi_{1i} + \frac{1}{k_{3i}}\xi_{2i} \tag{37}$$

Here, the functions $P_1(t)$ and $P_2(t)$ are defined as:

$$P_1(t) = \boldsymbol{\beta}_1^{\mathrm{T}}\left|\boldsymbol{z}_2(0)\right| - \boldsymbol{z}_2^{\mathrm{T}}(0)\boldsymbol{N}_1(0) - \int_0^t L_1(\tau)\mathrm{d}\tau \tag{38}$$

$$P_2(t) = \boldsymbol{\beta}_2^{\mathrm{T}}\left|\boldsymbol{z}_3(0)\right| - \boldsymbol{z}_3^{\mathrm{T}}(0)\boldsymbol{N}_2(0) - \int_0^t L_2(\tau)\mathrm{d}\tau \tag{39}$$

$$L_1(t) = \boldsymbol{r}_1^{\mathrm{T}}\left[\boldsymbol{N}_2 - \boldsymbol{v}\left(\boldsymbol{z}_2\right)\boldsymbol{\beta}_1\right] \tag{40}$$

$$L_2(t) = \boldsymbol{r}_2^{\mathrm{T}}\left[\boldsymbol{N}_1 - \boldsymbol{v}\left(\boldsymbol{z}_3\right)\boldsymbol{\beta}_2\right] \tag{41}$$

From the above equations, it can be concluded that the functions $P_1(t)$ and $P_2(t)$ are always positive definite.

Theorem 2: By selecting sufficiently large and appropriate controller gain matrices $\boldsymbol{k}_1$, $\boldsymbol{k}_2$, $\boldsymbol{k}_3$, $\boldsymbol{k}_{\mathrm{r}1}$, and $\boldsymbol{k}_{\mathrm{r}2}$, the following matrix:

$$\mathbf{\Lambda}=\begin{bmatrix} \boldsymbol{k}_1 & -\frac{\mathbf{I}_{6\times 6}}{2} & \mathbf{0}_{6\times 6} & \mathbf{0}_{6\times 6} & \mathbf{0}_{6\times 6} \\ -\frac{\mathbf{I}_{6\times 6}}{2} & \boldsymbol{k}_2 & -\frac{\mathbf{I}_{6\times 6}}{2} & \mathbf{0}_{6\times 6} & \mathbf{0}_{6\times 6} \\ \mathbf{0}_{6\times 6} & -\frac{\mathbf{I}_{6\times 6}}{2} & \boldsymbol{k}_{\mathrm{r}1} & \mathbf{0}_{6\times 6} & \mathbf{0}_{6\times 6} \\ \mathbf{0}_{6\times 6} & \mathbf{0}_{6\times 6} & \mathbf{0}_{6\times 6} & \boldsymbol{k}_3 & -\frac{\mathbf{I}_{6\times 6}}{2} \\ \mathbf{0}_{6\times 6} & \mathbf{0}_{6\times 6} & \mathbf{0}_{6\times 6} & -\frac{\mathbf{I}_{6\times 6}}{2} & \boldsymbol{k}_{\mathrm{r}2} \end{bmatrix} \tag{42}$$

is always positive definite. Then, the designed controller is semi-globally asymptotically stable and ensures that all signals in the closed-loop system are bounded, i.e., $\|z_1\|_\infty = \max\left(|z_{11}|,|z_{12}|,\cdots,|z_{1n}|\right)\to 0$, $t\to\infty$.
The proof process can be referred to in [17].

5. SIMULATION RESULTS

This section verifies the advancement and effectiveness of the designed multidimensional neural network-based integral robust controller for hydraulic manipulators through a simulation example of a three-DOF hydraulic manipulator wrist system. The system parameters are consistent with those in [18]. The structure of the three-DOF hydraulic manipulator wrist system is shown in Figure 3.

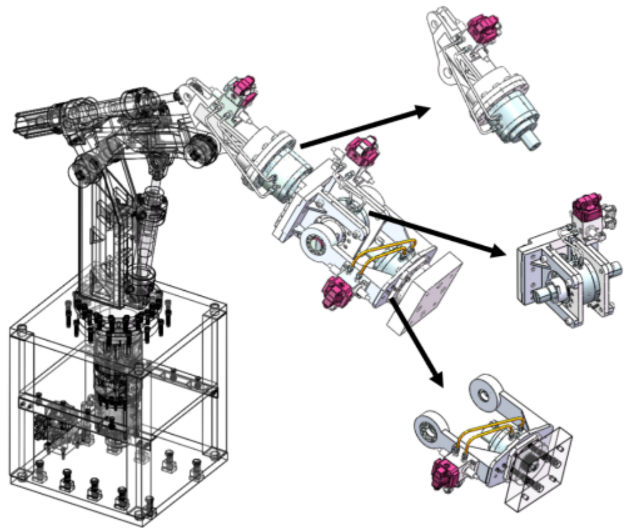

Figure 3 Schematic Diagram of The Hydraulic Manipulator Wrist Structure
To verify the fitting performance of the neural network, matched and unmatched uncertainties are designed as follows:

$$\begin{cases} \boldsymbol{\Delta}_{t1} = \dot{\boldsymbol{x}}_{1d} + \begin{bmatrix} 50 \\ 50 \\ 50 \end{bmatrix} \\ \boldsymbol{\Delta}_{t2} = \begin{bmatrix} 2\times10^4 \sin(0.5t) \\ 1\times10^4 \sin(0.5t) \\ 1\times10^4 \sin(0.5t) \end{bmatrix} \end{cases} \tag{43}$$

To compare the differences in simulation results under different controllers, the controller parameters are set as follows:

(1) Multidimensional Neural Network-Based Integral Robust Controller (C1): This is the controller proposed in this study. Its gains are: $\boldsymbol{k}_1 = \mathrm{diag}\{60,20,20\}$, $\boldsymbol{k}_2 = \mathrm{diag}\{500,800,500\}$, $\boldsymbol{k}_3 = \mathrm{diag}\{60,80,80\}$, $\boldsymbol{k}_{r1} = \mathrm{diag}\{4,5,4\}$, $\boldsymbol{k}_{r2} = \mathrm{diag}\{10,5,10\}$, $\boldsymbol{k}_s = \mathrm{diag}\{10,5,10\}$, $\boldsymbol{\beta}_1 = [8,2,1]^{\mathrm{T}}$, $\boldsymbol{\beta}_2 = [1000,100,150]^{\mathrm{T}}$, $H=16$, $L=12$, $\Gamma_{1i}=25$, $\Gamma_{2i}=20$.

(2) Feedback Linearization Controller (C2): This is a feedback linearization pose controller. Apart from the parameters not included, other controller gains remain the same as in C1.

The initial tracking command signals for each joint are:

$$\boldsymbol{x}_{1d} = \begin{bmatrix} 0.25\sin(0.5t)\times\left(1-e^{-0.01t^3}\right) \\ 0.20\sin(0.5t)\times\left(1-e^{-0.01t^3}\right) \\ 0.25\sin(0.5t)\times\left(1-e^{-0.01t^3}\right) \end{bmatrix} \tag{44}$$

The simulation results are shown in the following figures. Figure 4 shows the tracking control performance of each joint of the hydraulic manipulator wrist under different controllers. Figure 5 displays the tracking error results for Joint 1 under the two controllers. Figure 6 compares the tracking errors for Joint 2 under different controllers. Figure 7 shows the errors for Joint 3 under the two controllers.

From Figure 4, it can be observed that both controllers, C1 and C2, enable each joint to track the command signal (46) well, with no significant visual difference. However, Figures 5 to 7 more clearly demonstrate the tracking performance of the two controllers. Since the command signal exhibits periodic fluctuations, significant error fluctuations are observed during each hydraulic motor reversal due to the influence of unmodeled errors such as friction and disturbances. Controller C2 is a classic feedback linearization controller. However, lacking disturbance approximation and compensation capabilities, its tracking performance is noticeably inferior to that of the C1 neural network integral robust controller during simulation startup and reversal phases. This verifies the effectiveness of the proposed control strategy.

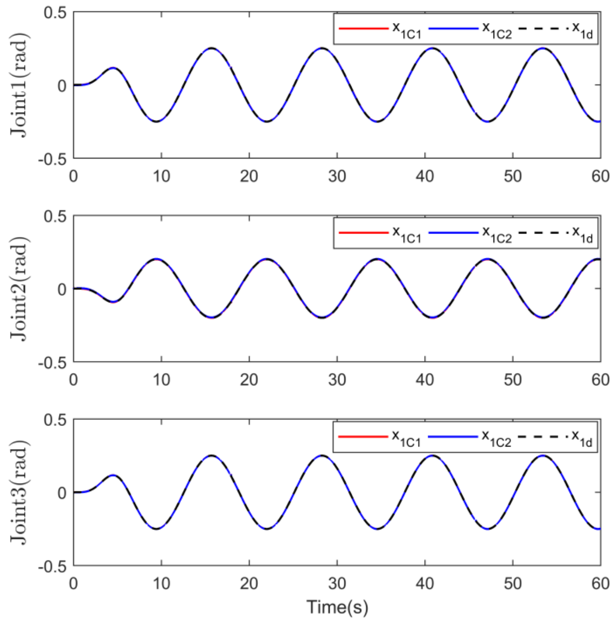

Figure 4 Tracking Effect Diagrams of Each Joint

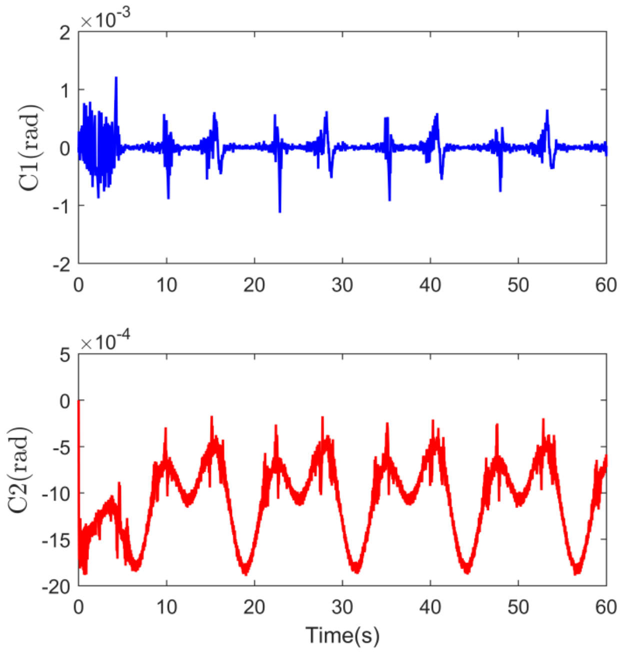

Figure 5 Comparison of Tracking Errors of Joint 1 Under Different Controllers

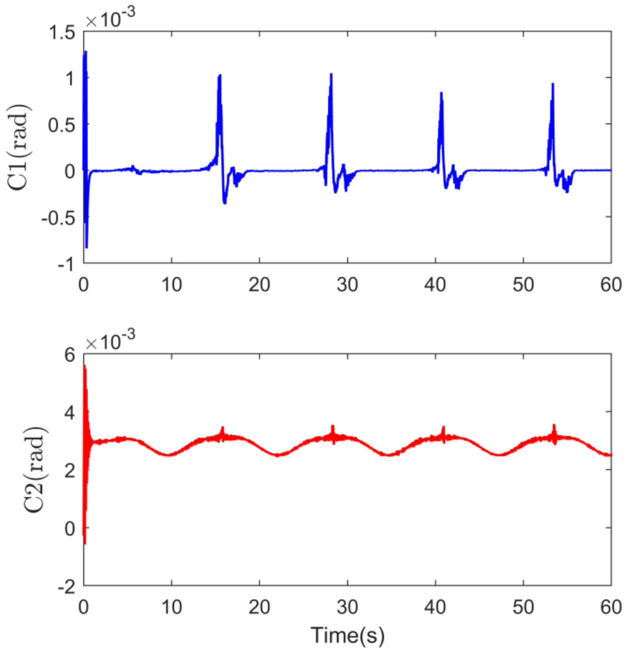

Figure 6 Comparison of Tracking Errors of Joint 2 Under Different Controllers

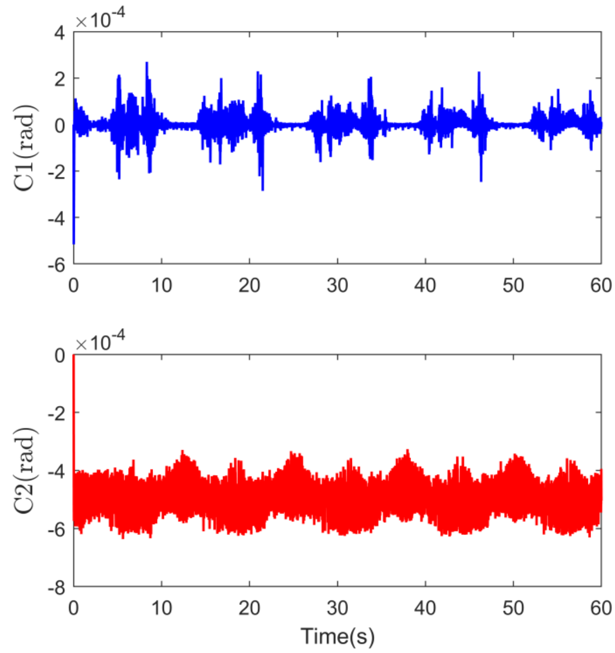

Figure 7 Comparison of Tracking Errors of Joint 3 Under Different Controllers

6. CONCLUSION

With the increasing demand for automation and intelligence in heavy-load operations, higher requirements are placed on the comprehensive control performance of hydraulically driven multi-DOF manipulators. Addressing major problems such as large model errors, high operational risks, and poor pose positioning accuracy in heavy-load hydraulic manipulator control, this study proposes an integral robust control strategy integrated with neural networks, achieving the approximation and compensation of unmodeled uncertainties. The main conclusions are as follows:

This study provides a robust and dynamically compensated solution for high-precision, high-reliability pose tracking control of heavy-load multi-DOF hydraulic manipulators, offering a new approach for high-performance controller design in complex scenarios.

7. REFERENCES

[1] GUO Qing. Development of Nonlinear Control Technology for Electro-hydraulic Servo System [J]. Chinese Hydraulics & Pneumatics,2018,(3): 1-9.

[2] Merritt H E. Hydraulic control systems[M]. New York: Wiley,1967.

[3] YAO Jianyong, JIAO Zongxia, MA Dawei, et al. High-accuracy tracking control of hydraulic rotary actuators with modeling uncertainties[J]. IEEE/ASME Transactions on Mechatronics, 2014, 19(2): 633-641.

[4] WANG Tianlei, WANG Chenxu, XIN Zengmiao, et al. Research on Reinforcement Learning-based Sliding Mode Control for Hydraulic Position Servo Systems[J]. Chinese Hydraulics & Pneumatics, 2025, 49(11):88-97.

[5] FU Xiang, WANG Ranfeng, ZHAO Yangsheng. Self-adaptive control method of fluid feeding with steady pressure for hydraulic support based on overlapping synergetic logic[J]. Journal of China Coal Society, 2020, 45(5):15-25.

[6] WANG Chengwen, JIAO Zongxia, WU Shuai, et al. Nonlinear adaptive torque control of electro-hydraulic load system with external active motion disturbance[J]. Mechatronics, 2014,24(1): 32-40.

[7] LIU Haodong, LI Shizhen, SHI Wenzhuo. Model Predictive Control of Offshore Gangway Hydraulic System Based on Extended State Observer[J]. Chinese Hydraulics & Pneumatics, 2024, 48(9): 22-29.

[8] MA Yanbin, ZHAO Bin, HAO Yunxiao. Characteristics Analysis of Asymmetric Pump-controlled Single-rod Hydraulic Cylinder System[J]. Chinese Hydraulics & Pneumatics, 2023,47(1): 70-76.

[9] JI Hong, ZHAO Hongke, LIU Yaozhuo, et al. Backflushing Jet and Flow Loss in Distribution Valve of Water Piston Pump [J]. Chinese Hydraulics & Pneumatics, 2022, 46(11): 1-8.

[10] Xia Yangxiu, Qi Manzhi, et al. Advanced Motion Control of Hydraulic Manipulator With Precise Compensation of Dynamic Friction[J]. IEEE Transactions on Industrial Informatics, 2024, 20(7): 9375-9384.

[11] Zhang Han, Liu Yuhan, Zhan Liaoyang, et al. A Human–Machine Cooperative Control Strategy Based on Deep Reinforcement Learning to Enhance Heavy Vehicle Driving Safety[J]. IEEE Transactions on Human-Machine Systems, 2025, 55(6): 1006-1015.

[12] ZHANG Jiarui, GE Lei, HAO Yunxiao. Discrete PID Control of Closed Pump Control Hydraulic-mechanical Linear Actuator[J]. Chinese Hydraulics & Pneumatics, 2024,48(9): 54-60.

[13] YAO Zhikai, LIANG Xianglong, JIANG Guoping, et al. Model-Based Reinforcement Learning Control of Electrohydraulic Position Servo Systems[J]. IEEE/ASME Transactions on Mechatronics, 2023, 28(3): 1446-1455.

[14] ZHANG Luyao, WANG Haolin, XIA Wanrun, et al. Scaled Gain-Based Extended State Observer for Disturbed Systems With Time-Varying Delays[J]. IEEE Transactions on Circuits and Systems II: Express Briefs, 2026, 73(1): 68-72.

[15] ZHU Yukai, QIAO Jianzhong, GUO Lei. Adaptive sliding mode disturbance observer-based composite control with prescribed performance of space manipulators for target capturing[J]. IEEE Transactions on Industrial Electronics, 2020,67(4): 3083-3093.

[16] ZHENG Yuyan, MI Junjie, SHEN Gang. Dual RISE Control for Multi-Degree-of-Freedom Hydraulic Manipulator with Prescribed Performance Function[J]. Chinese Hydraulics & Pneumatics, 2025, 49(6):102-111.

[17] DENG Wenxiang, ZHOU Hang, ZHOU Jin, et al. Neural Network-Based Adaptive Asymptotic Prescribed Performance Tracking Control of Hydraulic Manipulators. IEEE Transactions on Systems, Man, and Cybernetics: Systems, 2023, 53(1):285-295.

[18] MI Junjie, DENG Wenxiang, YAO Jianyong,et al. Linear-Extended-State-Observer-Based Adaptive RISE Control for the Wrist Joints of Manipulators with Electro-Hydraulic Servo Systems[J]. Electronics, 2024, 13(6).

Biographies

Junjie Mi received the B.Tech degree in vehicle engineering from the College of Economics and Technology, Anhui Agricultural University, Hefei, China, in 2017, and the Ph.D. degree in mechatronic control from the Nanjing University of Science and Technology, Nanjing, China, in 2024. In 2024, he joined the School of Mechatronics Engineering, Anhui University of Science and Technology, Huainan, China, as an Lecturer. In 2025, he joined the State Key Laboratory of Digital Intelligent Technology for Unmanned Coal Mining, Huainan, China. His current research interests include electro-hydraulic servo control, hydraulic manipulators, and disturbance rejection control.

Gang Shen received the M.Sc. and Ph.D. degrees in mechanical engineering from the Harbin Institute of Technology, Harbin, China, in 2007 and 2011, respectively. In 2023, he joined the School of Mechatronics Engineering, Anhui University of Science and Technology, Huainan, China. In 2025, he joined the State Key Laboratory of Digital Intelligent Technology for Unmanned Coal Mining, Huainan, China. He is currently working as a Full Professor**.** Dr. Shen current research interests include servo control of mechatronic systems, parallel robot, and adaptive control.

Jianyong Yao received the B. Tech degree in mechatronics from Tianjin University, Tianjin, China, in 2006, and the Ph.D. degree in mechatronic engineering from Beihang University, Beijing, China, in 2012. He was a visiting exchange student with the School of Mechanical Engineering, Purdue University, from Oct. 2010 to Oct. 2011. In 2012, he joined the School of Mechanical Engineering, Nanjing University of Science and Technology, Nanjing, China, and currently as a Full Professor. Dr. Yao current research interests include servo control of mechatronic systems, adaptive and robust control, fault detection and accommodation of dynamic systems.